

INVESTIGATION OF THE PERFORMANCE CHARACTERISTICS OF 500 NM TO 510 NM GREEN InGaN MQWs LASER DIODES

GH. ALAHYARIZADEH^{a*}, Z. HASSAN^a, S.M. THAHAB^b, F. K. Yam^a

^a*Nano-Optoelectronics Research and Technology Laboratory, School of Physics,
Universiti Sains Malaysia, 11800- Penang, Malaysia*

^b*Material Engineering Department, College of Engineering, University of Kufa,
Najaf, Iraq*

The performance characteristics of green InGaN multi-quantum well laser diode structures emitting at 500 nm to 510 nm were investigated numerically. A threshold current of 87.2 mA corresponding to the threshold current density of 4.84 kA/cm² and a threshold voltage of 8.837 V were achieved for a basic structure emitting at 504.31 nm output emission wavelength. The effects of well numbers, well thickness, barrier thickness, and barrier doping on performance characteristics such as output power, threshold current, slope efficiency, and differential quantum efficiency were studied. The basic structure and material parameters used in the model were extracted based on the newest literatures and experimental works. Simulation results indicated that lowest threshold current, highest output power, differential quantum efficiency and slope efficiency are observed when the number of well layers is one and well thickness is between 3 and 4 nm. Significant changes in output power, threshold current, and slope efficiency were observed with the variations in barrier thickness and doping.

(Received January 16, 2013; Accepted March 15, 2013)

Keywords: Quantum well, InGaN green laser, Well number, Well thickness,
Numerical simulation.

1. Introduction

In recent years, III-nitride-based green semiconductor lasers have attracted much attention due to their promising application in mobile full colour projectors that employ red, green and blue laser diodes as light sources, which are poised for introduction into the market in the coming years [1–3]. Although second harmonic generation green laser diodes have already been introduced into the market, AlInGaN-based green semiconductor lasers offer the promise of reduced build-up costs, compactness, access to a wider wavelength range, and increased efficiency and reliability [1–3].

After the first manifestation of blue III-nitride semiconductor lasers by Nakamura et al. [5], several groups such as Ryu et al. [6], Kuo et al. [7], and others investigated and developed nitride semiconductor lasers to reach lower (violet and ultraviolet) and longer (green) wavelengths experimentally and theoretically using different equipment and methods separately [6–10]. To follow this trend, in recent years, several researchers have published their results on longer wavelength laser diodes at 500 nm to 530 nm [1–5, 11–16]. Although these laser diodes have been realized by several groups, InGaN green lasers is an emerging subject, and few studies have been carried out in terms of carrier behaviour and investigation of structural, optical, and electrical parameters affecting laser performance. Furthermore, the tendency of green laser diodes to reach greater performance and lower threshold current encourages researchers to continue investigating these diodes theoretically and experimentally.

* Corresponding author: g_alahyarizadeh@yahoo.com

In the current research, the performance characteristics of green InGaN multi-quantum well (MQW) laser structures with output emission wavelengths around 500 nm to 510 nm were investigated using Integrated System Engineering Technical Computer Aided Design (ISE TCAD) software. The distribution of electron and hole carrier densities and radiative recombination, as well as their roles on laser performance for different well numbers and thicknesses were also presented. The effects of barrier thickness and doping on performance characteristics of green InGaN laser were likewise investigated.

2. Laser structure and simulation parameters

The basic laser structure under study was extracted from a real laser structure fabricated by Adachi et al., which was grown through metal organic chemical vapour deposition [1, 2]. As shown in Fig. 1., the laser structure includes an n-type GaN layer, an n-type $\text{In}_{0.1}\text{Ga}_{0.9}\text{N}$ compliance layer, an n-type $\text{Al}_{0.12}\text{In}_{0.032}\text{GaN}$ quaternary cladding layer, an n-type GaN waveguiding layer, an InGaN/InGaN MQW active region, a p-type $\text{Al}_{0.2}\text{Ga}_{0.8}\text{N}$ electron blocking layer (EBL), a p-type GaN waveguiding layer, a p-type $\text{Al}_{0.12}\text{In}_{0.032}\text{GaN}$ quaternary cladding layer, and a p-type GaN contact layer [1, 2]. The MQW active region was selected based on Nakamura et al., which consists of three 4 nm $\text{In}_{0.3}\text{Ga}_{0.7}\text{N}$ wells sandwiched between four 10 nm $\text{In}_{0.03}\text{Ga}_{0.97}\text{N}$ barriers [3]. The doping concentrations of n- and p-type layers are $1\text{e}18$ and $5.5\text{e}18$, respectively. The laser area is $3 \mu\text{m} \times 600 \mu\text{m}$, and the reflectivities of the back and front mirrors are equal to 80% and 95%, respectively [1,2].

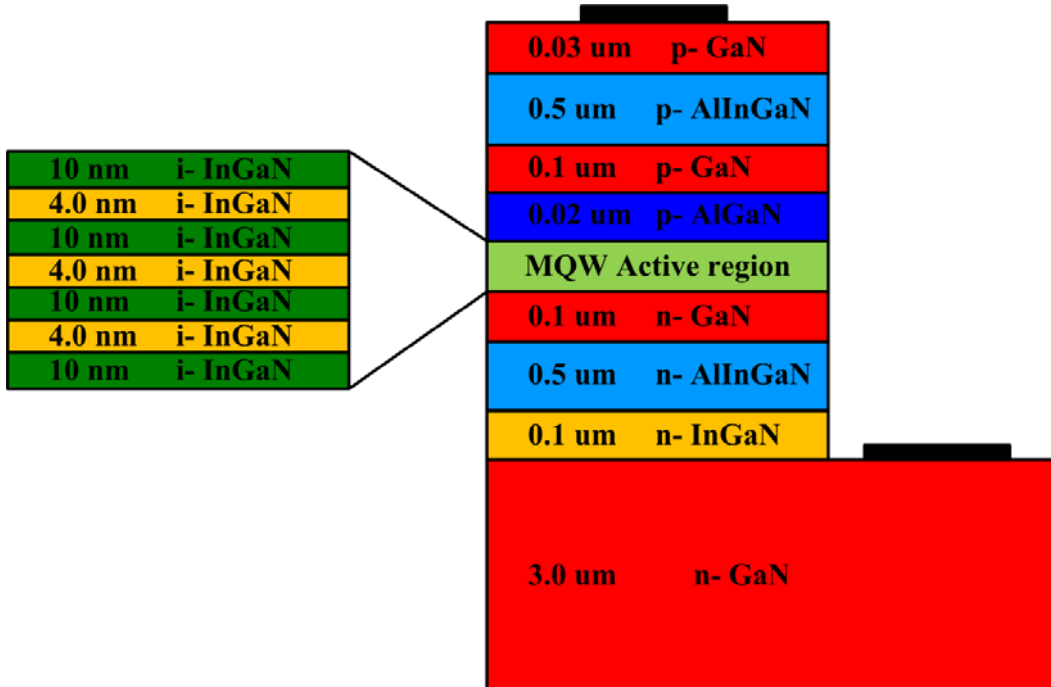


Fig. 1. Schematic diagram of the green InGaN MQW laser structure under study.

The laser simulation was carried out by solving several equations, including Poisson equation, Schrodinger equation, current continuity equations, photon rate equation, and scalar wave equation, using the two-dimensional ISE TCAD simulator. This simulator also involves the carrier drift-diffusion model that contains Fermi statistics and incomplete ionization [9,17].

The physical parameters of all ternary and quaternary alloys used in the simulation were interpolated by binary alloys that can be expressed by the following equation:

$$Q_{\text{Al}_x\text{In}_y\text{Ga}_{1-x-y}\text{N}} = x \cdot Q_{\text{AlN}} + y \cdot Q_{\text{InN}} + (1 - x - y) \cdot Q_{\text{GaN}}, \quad (1)$$

where Q_{InN} , Q_{GaN} , and Q_{AlN} are the physical parameters of InN, GaN, and AlN, such as effective masses, refractive index, and others as listed in Table 1 [9,17]. The above equation applies to all physical parameters except for band gap energy, which can be expressed by the following equations [9,17,18]:

$$E_g(AlInGaN) = \frac{xyE_g^u(AlInN) + yzE_g^v(InGaN) + xzE_g^w(AlGaN)}{xy + yz + zx}, \quad (2)$$

$$E_g^u(AlInN) = u \cdot E_g(AlN) + (1-u) \cdot E_g(GaN) - u \cdot (1-u)b(AlInN), \quad (3)$$

$$E_g^v(InGaN) = v \cdot E_g(GaN) + (1-v) \cdot E_g(AlN) - v \cdot (1-v)b(AlGaN), \quad (4)$$

$$E_g^w(AlGaN) = w \cdot E_g(AlN) + (1-w) \cdot E_g(GaN) - w \cdot (1-w)b(AlGaN), \quad (5)$$

$$u = \frac{1-x+y}{2}, \quad v = \frac{1-y+z}{2}, \quad w = \frac{1-x+z}{2}, \quad (6)$$

where x , y , and $z=1-x-y$ are the compositions of aluminum, indium, and gallium in the AlInGaN, respectively. $E_g(AlN)$, $E_g(GaN)$, and $E_g(AlN)$ are the band gap energies of InN, GaN, and AlN, respectively, while $b(AlInN)$, $b(AlGaN)$, and $b(AlGaN)$ are band gap bowing parameters of AlInN, InGaN, and AlGaN which are 2.5, 1.4, and 0.7, respectively [17,18]. The parameters of the binary materials used in this work are listed in Table 1 [17,18].

Table 1. Room temperature properties of binary III-N materials [17]

Parameters	GaN	AlN	InN
Bandgap energy E_g (eV)	3.47	6.28	0.8
Electron affinity (eV)	4.1	1.9	5.8
Lattice constant a_o (\AA)	3.189	3.112	3.545
Refractive index near E_g	2.506	2.035	2.9
Electron effective mass	$0.22 m_e$	$0.4 m_e$	$0.11 m_e$
Heavy hole effective mass	$1.595 m_e$	$2.68 m_e$	$1.449 m_e$
Light hole effective mass	$0.261 m_e$	$0.261 m_e$	$0.157 m_e$

3. Simulation results and discussion

Light output characteristics ($L-I$) and peak emission wavelength of the basic green InGaN MQW laser diode (LD) are shown in Figs. 2 and 3, respectively. As shown in Fig. 2, the threshold current of LD is 87.2 mA, which corresponds to the threshold current density of 4.84 kA/cm². The threshold voltage of LD is also 8.837 V. The obtained results are in good agreement with the experimental results observed by Adachi et al. [1 and 2]. The peak emission wavelength (504.31 nm) of green InGaN MQW LD is shown in Fig. 3, which is also in good agreement with the output emission wavelength of the laser structure fabricated by Tyagi et al. [3].

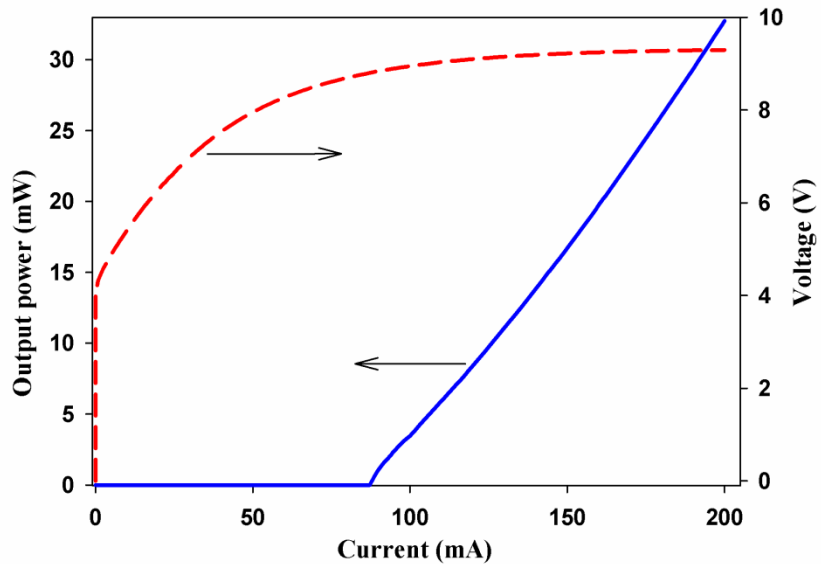


Fig. 2. Light output characteristic ($L-I$) of the basic green InGaN MQW laser

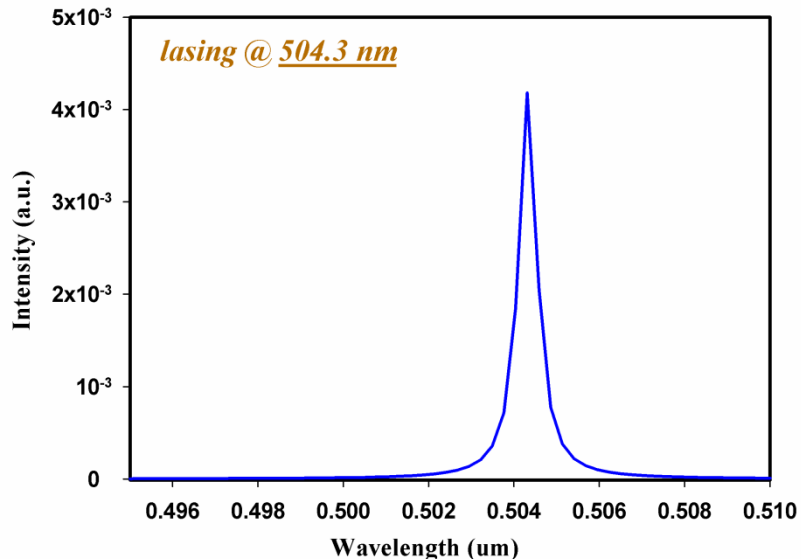


Fig. 3. Peak emission wavelength of the basic green InGaN MQW laser

Fig. 4 shows the optical intensity and refractive index profile of the basic green InGaN MQW LD. As shown in the figure, maximum optical intensity occurs in the active region due to the optical confinement obtained by the GaN waveguide and the AlInGaN quaternary cladding layers.

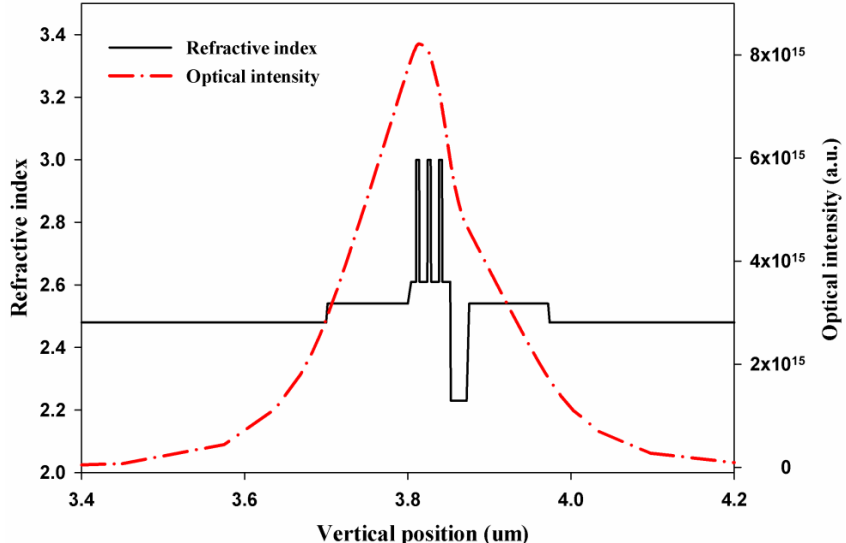


Fig. 4. Optical intensity of the basic green InGaN MQW laser

The first geometrical parameter that affects the performance characteristics of MQW laser is cavity length. Several performance characteristics such as threshold current, differential quantum efficiency (DQE), output power, internal quantum efficiency, and internal loss depend on cavity length. Fig. 5 shows the threshold current and DQE of green InGaN MQW LD as a function of cavity length. As shown in this figure, decreasing cavity length causes DQE to increase and threshold current to decrease. These results could be related to the increase in the power consumption of the structure due to the increase in cavity length and laser structure. Thus, the laser with a longer cavity length requires a higher current to start lasing and, consequently, has a higher threshold current.

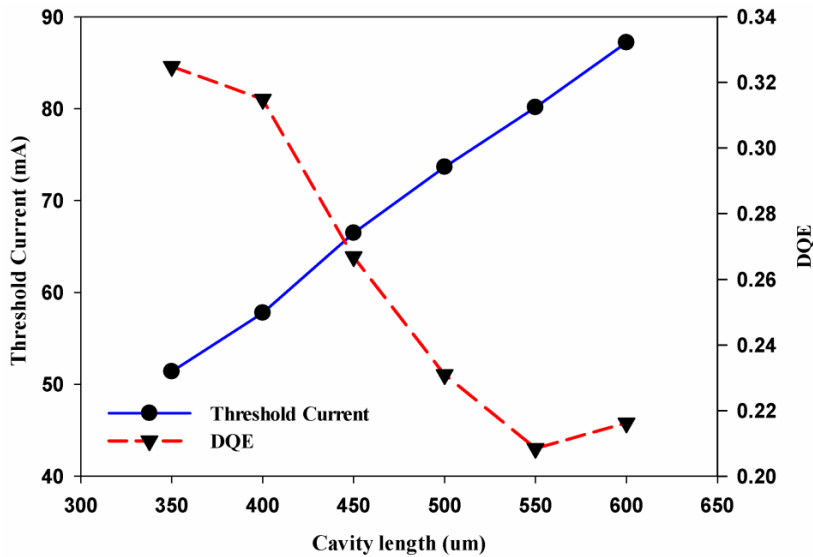


Fig. 5. Threshold current and DQE of the basic green InGaN MQW laser as a function of cavity length

Fig. 6 shows the threshold current, output power, slope efficiency, and DQE of green MQW laser diodes with various well numbers. As shown in the figure, the lowest threshold current and highest output power, slope efficiency, and DQE were observed when well number was one. It can be due to that the second and third quantum well could have been dissociated during the growth and lose their crystal quality which cause to increase the internal loss and decrease the performance characteristics. The obtained results are compatible with the experimental results presented by Sizov et al. [4, 16]. Earlier studies on the performance of III-

nitride semiconductor lasers with different emission wavelengths of 390 nm to 420 nm and longer than 435 nm were conducted experimentally and theoretically by several groups, including Nakamura et al., Ryu et al., Kuo et al., and others. They demonstrated that for emission wavelengths between 390 and 420 nm, the lowest threshold current density was obtained when the number well layers was two. However, in another study, they found that for emission wavelengths longer than 435 nm, the lowest threshold current density was obtained when the number of well layers was one or three, and increased with the increase in the number of well layers. The displayed results in Fig. 6 indicate that green emission wavelengths can be considered as following emission wavelengths longer than 435 nm.

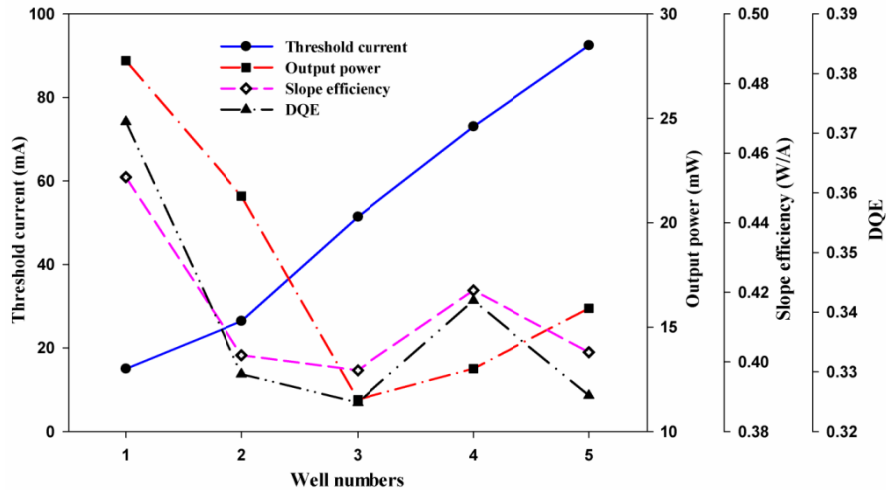


Fig. 6. Threshold current, output power, slope efficiency and DQE of the green InGaN MQW lasers as a function of number of wells.

Fig. 7 shows the radiative recombination rate for laser structures with different numbers of wells. As shown in this figure, increasing the number of wells resulted in a decrease in radiative recombination rate level. The highest radiative recombination also occurred in the well close to the p-side. The highest carrier density was found in the well close to the p-side due to the use of thin layer EBL after the last barrier in p-side. The radiative recombination in the well close to the n-side was also higher than others due to its higher electron density.

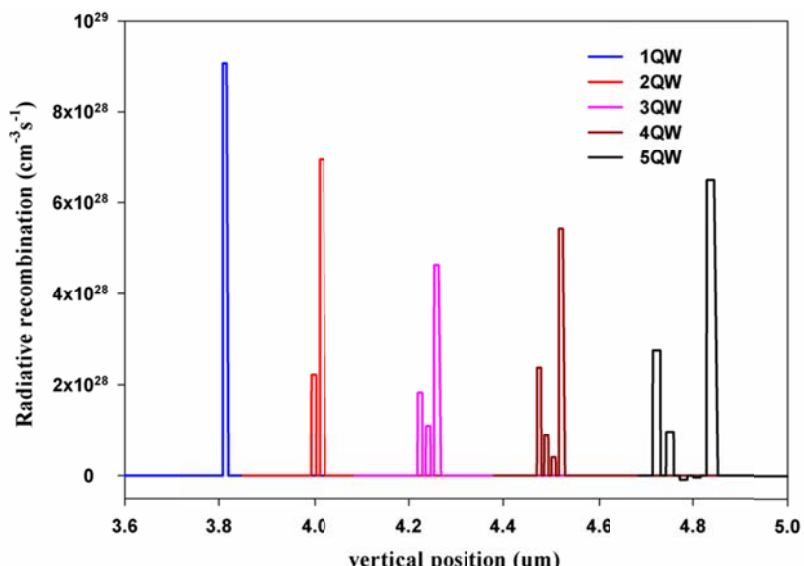


Fig. 7. Radiative recombination rate for green InGaN MQW LDs with different number of wells

threshold current, output power and DQE of green InGaN single quantum well (SQW) lasers as functions of well thickness is shown in Fig. 8. The figure indicates that increasing well thickness led to a decrease in output power. It could be related to the decrease in electron and hole carrier densities and consequently, decrease in radiative recombination in the well due to the increase in well thickness. Fig. 9 shows the electron and hole carrier densities and radiative recombination of green InGaN SQW laser as a function of well thickness. Fig. 8 also shows that the lower threshold current and higher DQE could be obtained when the well thickness is between 3 and 4 nm. The threshold current is highly dependent on quantum well thickness because of the quantum confined stark effect (QCSE) and the exciton localization effect. The obtained results indicate that QCSE dominated the recombination emission in the wide quantum well structure, whereas the exciton localization effect dominated the recombination emission in the thin quantum well structure. Achieved results were also in good agreement with the experimental works done by Nakamura et al. [5].

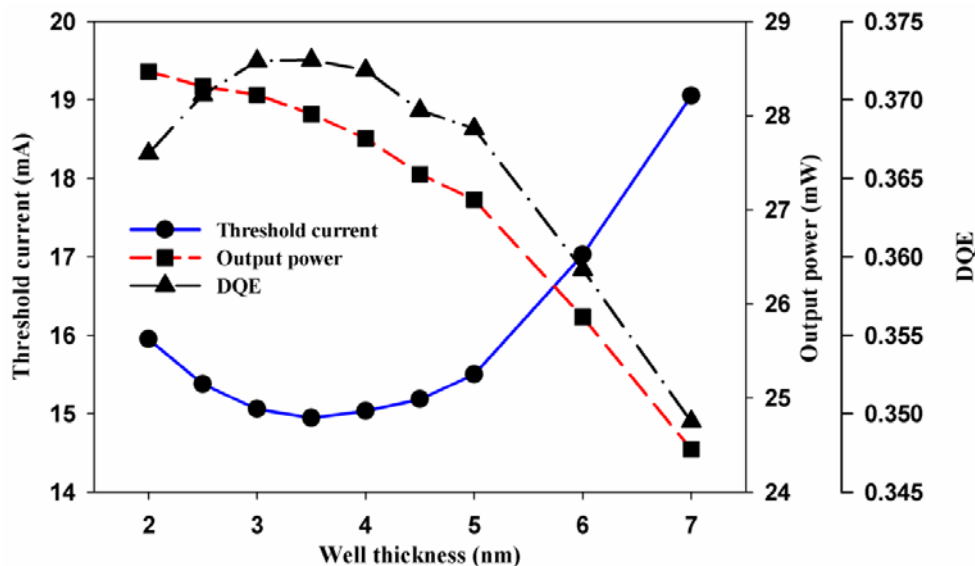


Fig. 8. Threshold current, output power and DQE of the green InGaN SQW lasers as a function of well thickness.

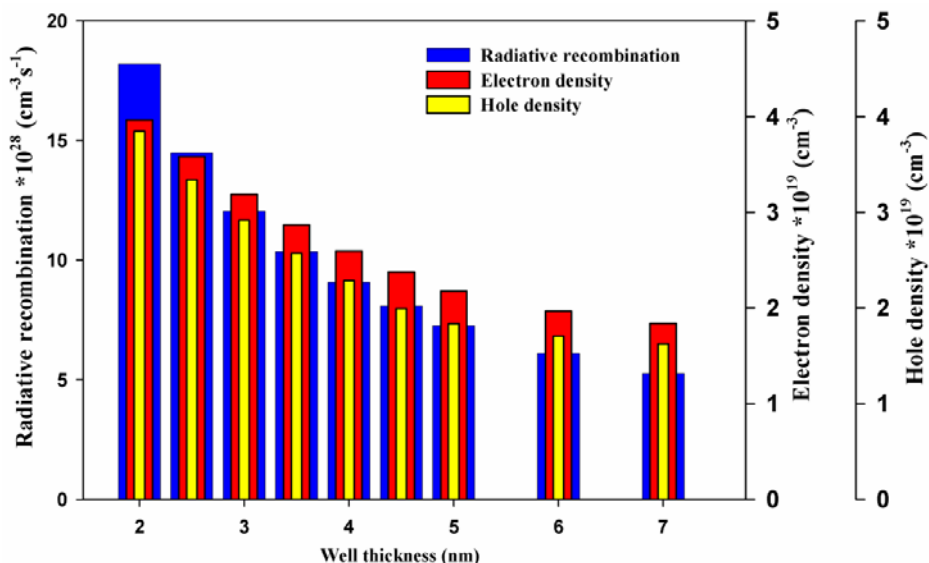


Fig. 9. Electron and hole carrier densities and radiative recombination of the green InGaN SQW laser as a function of well thickness.

Fig. 10 shows the peak emission wavelength and optical confinement factor (OCF) of green InGaN SQW LDs as a function of well thickness. The figure shows that increasing well thickness caused the active region surface and the OCF to increase. Note that increasing well thickness caused an increase in peak emission wavelength. As a result, the transition energies between electrons and holes in the conduction and valence bands, and consequently peak emission wavelength, shifted toward the red spectrum by increasing well thickness.

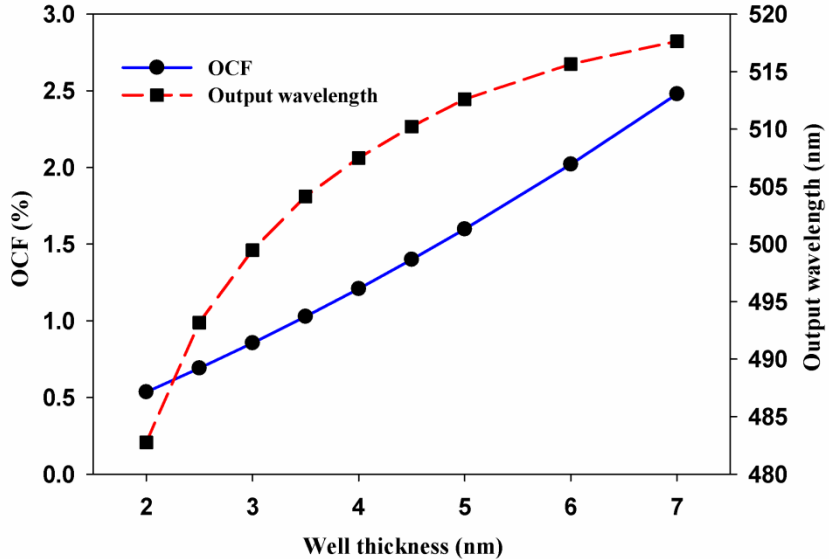


Fig. 10. Peak emission wavelength and OCF of the green InGaN SQW LDs as a function of well thickness

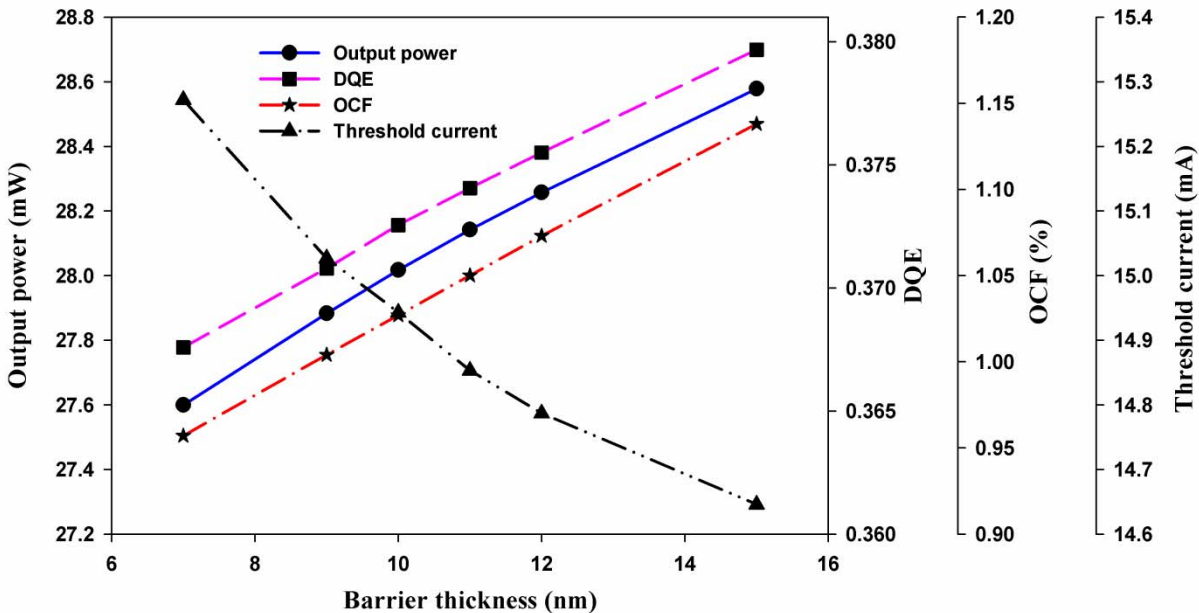


Fig. 11. Threshold current, output power, DQE and OCF of the green InGaN SQW lasers as a function of barrier thickness

Fig. 11 shows the dependence of threshold current, output power, DQE, and OCF of the green InGaN SQW laser diodes for various barrier thicknesses. As shown in the figure, higher barrier thickness caused better optical confinement and better radiative recombination, and consequently, higher output power and DQE. The obtained results are in good agreement with the experimental work done by Nakamura et al. [5]. Moreover, a higher output power for a wider

barrier could be related to the shorter emission wavelength for a wider barrier, which results in higher DQE.

The dependence of threshold current and output power of green InGaN SQW LD on barrier doping concentration is shown in Fig. 12. As shown in this figure, increasing the doping concentration in the barrier caused a decrease in threshold current and an increase in output power. Increasing output power by increasing the doping concentration could be related to the increase in radiative recombination in the well. Fig. 13 shows the electron and hole densities and radiative recombination rate in the well of green InGaN SQW LD as functions of barrier doping concentration.

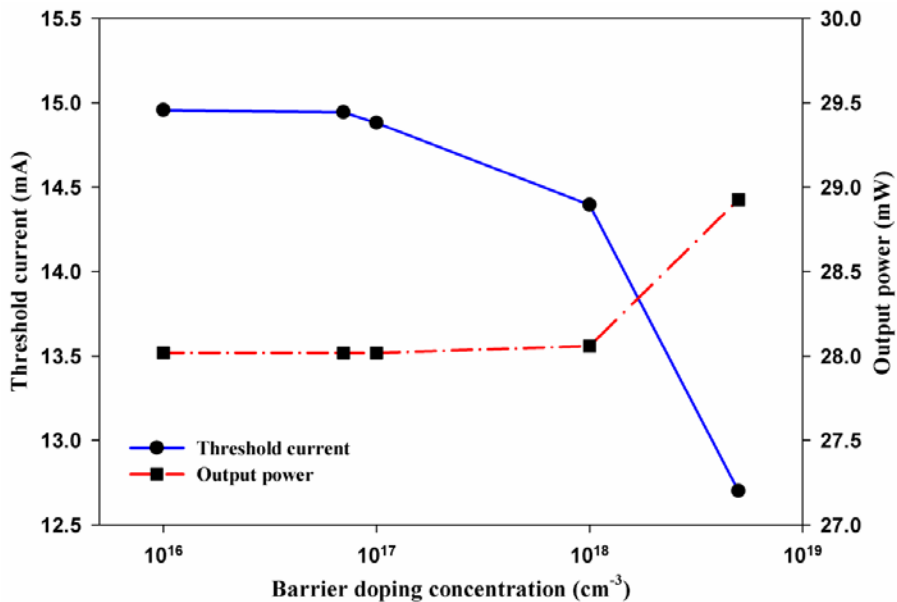


Fig. 12. Threshold current and output power of the green InGaN SQW lasers as a function of barrier doping concentration

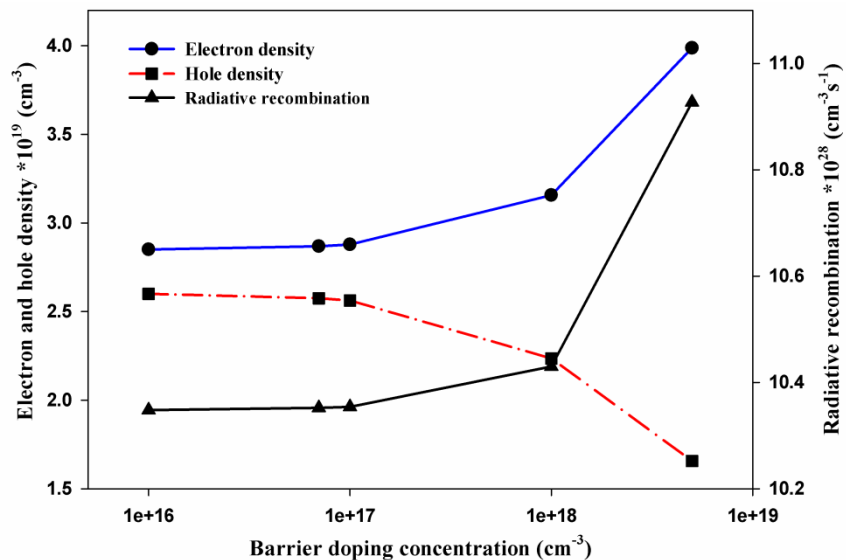


Fig. 13. Electron and hole densities and radiative recombination of the green InGaN SQW lasers as a function of barrier doping concentration.

Fig. 14 shows the bandgap, conduction- and valence-band energies and the electron and hole Fermi levels of the InGaN green SQW laser. The deformed conduction-band profile near the AlGaN EBL and the last InGaN barrier interface is due to the built-in polarization effects,

polarization charge densities and their corresponding electric fields which are inherent properties of III-nitride semiconductor devices. The highest bandgap energy region, EBL, allows more carriers to gather in the active region and increase the recombination rate. The EBL layer also reduces the electron current overflow from the active region to p side region. The GaN waveguide and the AlInGaN quaternary cladding layers which surrounded active region cause to carrier and optical confinements. The carrier confinement increases the radiative recombination rate and the optical confinement enhances the optical intensity and concentrates optical mode distribution in the active region. Fig. 15 shows the optical intensity and refractive index profile of the green InGaN SQW LD. As shown in the figure, maximum optical intensity occurs in the active region.

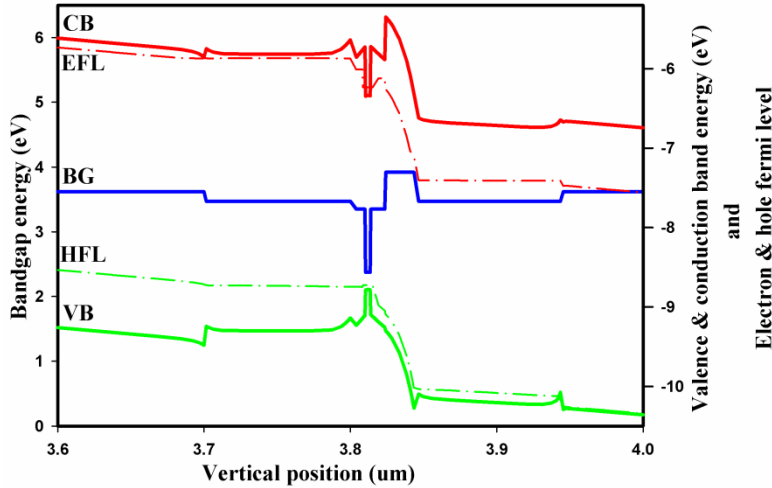


Fig. 14. Bandgap, conduction- and valence- band energies and electron and hole Fermi levels of the InGaN green SQW laser

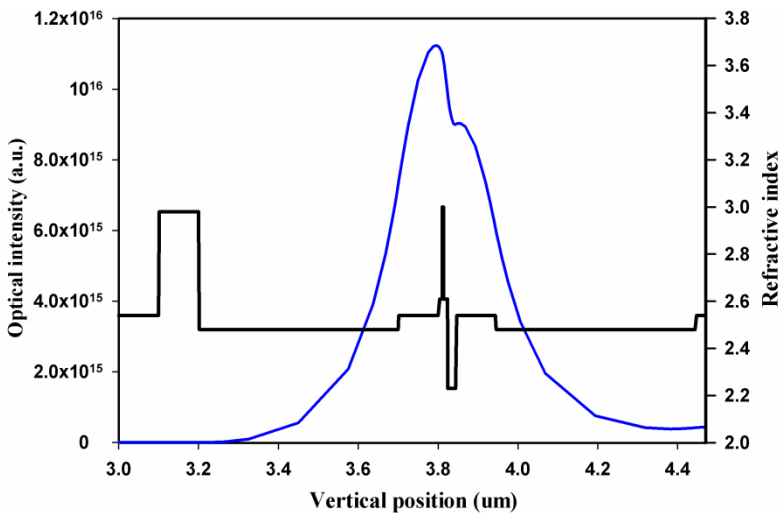


Fig. 15. Optical intensity and Refractive index profile of green InGaN SQW

Optical and lasing mode distribution of the optimized green InGaN SQW LD is shown in the Fig. 16. As shown in this figure, the greatest optical lasing mode distribution is in the active regions due to optical confinement which is provided by GaN waveguide and quaternary AlInGaN cladding layers.

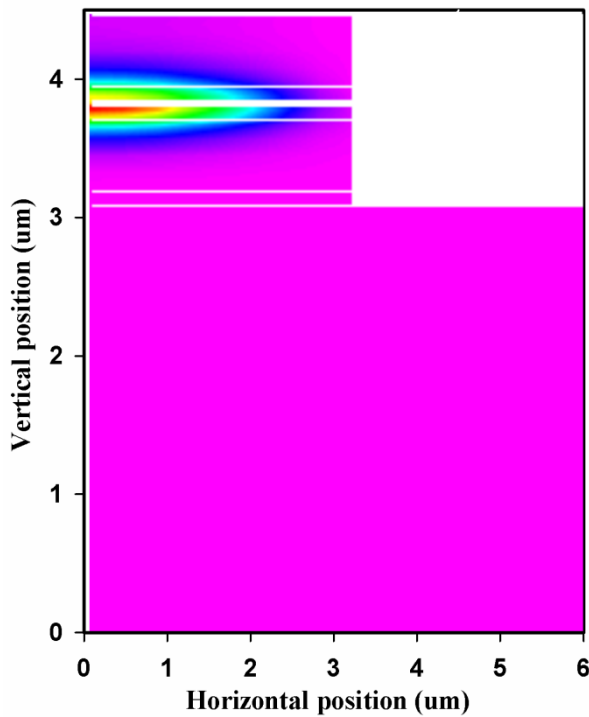


Fig. 16. Optical and lasing mode distribution of the optimized green InGaN SQW LD

4. Conclusion

A numerical simulation was carried out on green InGaN MQW laser diode structures emitting at 500 nm to 510 nm using ISE TCAD software. The effects of important structural and operating parameters such as cavity length, well numbers, well thickness, barrier thickness, and barrier doping on performance characteristics such as output power, threshold current, and slope efficiency were investigated. The results indicated that lowest threshold current, maximum output power, and slope efficiency can be obtained when the well number is one and well thickness is between 3 and 4 nm. They also indicated that variations in well and barrier thickness and barrier doping have a significant effect on output power, threshold current, slope efficiency, and DQE. Our results are in agreement with the experimental results observed by Adachi et al. [1 and 2], Tyagi et al. [3], and Sizov et al. [4].

Acknowledgment

The support from RU grant and Universiti Sains Malaysia is gratefully acknowledged.

References

- [1] Y. Yoshizumi, M. Adachi, Y. Enya, T. Kyono, S. Tokuyama, T. Sumitomo, K. Akita, T. Ikegami, M. Ueno, K. Katayama, T. Nakamura, *Applied Physics Express*, **2**(9), 092101 (2009).
- [2] M. Adachi, Y. Yoshizumi, Y. Enya, T. Kyono, T. Sumitomo, S. Tokuyama, S. Takagi, K. Sumiyoshi, N. Saga, T. Ikegami, M. Ueno, K. Katayama, T. Nakamura, *Applied Physics Express*, **3**, 121001 (2010).
- [3] A. Tyagi, R. M. Farrell, K. M. Klchner, C. Y. Huang, P. S. Hsu, D. A. Haeger, M. T. Hardy, C. Holder, K. Fujito, D. A. Cohen et al., *Applied Physics Express*, **3**, 011002 (2010).

- [4] D. S. Sizov, R. Bhat, A. Zakharian, S. Kechang, D. E. Allen, S. Coleman, Z. Chung-en, IEEE Journal of Selected Topics in Quantum Electronics, **17**, 1390 (2011).
- [5] Y.-D. Lin, A. Chakraborty, S. Brinkley, H. C. Kuo, T. Melo, K. Fujito, J. S. Speck, S. P. DenBaars, S. Nakamura, Applied Physics Letters, **94**, 261108 (2009).
- [6] H. Y. Ryu, K. H. Ha, J. K. Son, S. N. Lee, H. S. Paek, T. Jang, Y. J. Sung, K. S. Kim, H. K. Kim, Y. Park, and O. H. Nam, Applied Physics Letters, **93**, 011105 (2008).
- [7] Y. Chang and Y.K. Kuo, Journal of Applied Physics, **93**, 4992 (2003).
- [8] T. Lermer, A. Gomez-Iglesias, M. Sabathil, J. Muller, S. Lutgen, U. Strauss, B. Pasenow, J. Hader, J. V. Moloney, S. W. Koch, W. Scheibenzuber, U. T. Schwarz, Applied Physics Letters, **98**, 021115 (2011).
- [9] Gh. Alahyarizadeh, A. J. Ghazai, R. Rahmani, H. Mahmodi, Z. Hassan, Optics Communications, **285**, 746 (2012).
- [10] Y. K. Kuo, B. T. Liou, M. L. Chen, S. H. Yen, C. Y. Lin, Optics Communications, **231**, 395 (2004).
- [11] C.-Y. Huang, Y.-D. Lin, A. Tyagi, A. Chakraborty, H. Ohta, J. S. Speck, S. P. DenBaars, and S. Nakamura, Journal of Applied Physics, **107**, 023101 (2010).
- [12] D. Queren, A. Avramescu, G. Bruderl, A. Breidenassel, M. Schillgalies, S. Lutgen, U. Strauss, Applied Physics Letters, **94**, 081119 (2009).
- [13] A. Avramescu, T. Lermer, J. Muller, S. Tautz, D. Queren, S. Lutgen, U. Strauss, Applied Physics Letters, **95**, 071103 (2009).
- [14] T. Miyoshi, S. Masui, T. Okada, T. Yanamoto, T. Kozaki, S. Nagahama, T. Mukai, Applied Physics Express, **2**, 062201 (2009).
- [15] Y. Enya, Y. Yoshizumi, T. Kyono, K. Akita, M. Ueno, M. Adachi, T. Sumitomo, S. Tokuyama, T. Ikegami, K. Katayama, T. Nakamura, Applied Physics Express **2**(8), 082101 (2009).
- [16] D. S. Sizov, R. Bhat, A. Zakharian, J. Napierala, K. Song, D. Allen, C. Zah, Applied Physics Express, **3**, 122101 (2010).
- [17] Gh. Alahyarizadeh, Z. Hassan, S.M. Thahab, A.J. Ghazai, H. Mahmodi Journal of nanophotonics, **6**, 063514 (2012).
- [18] J.-R. Chen, C.-H. Lee, T.-S. Ko, Y.-A. Chang, T.-C. Lu, H.-C. Kuo, Y.-K. Kuo, S.-C. Wang, J. Lightwave Technol. **26**, 329 (2008).